Appl. Phys. B 70, 163–168 (2000) / Digital Object Identifier (DOI) 10.1007/s003409900108

Applied Physics B
Lasers
and Optics

Femtosecond noncollinear and collinear parametric generation and amplification in BBO crystal

V. Krylov[1], **J. Gallus**[1], **U.P. Wild**[1], **A. Kalintsev**[2], **A. Rebane**[3]

[1] Physical Chemistry Laboratory, Swiss Federal Institute of Technology, CH-8092 Zurich, Switzerland
(Fax: +41-1/632-1021, E-mail: krylov@phys.chem.ethz.ch)
[2] S.I. Vavilov State Optical Institute, 199034 St. Petersburg, Russia
(Fax: +7-812/393-1598, E-mail: agkalin@comset.spb.ru)
[3] Department of Physics, Montana State University, Bozeman, MT 59717, USA
(Fax: +1-406/994-4452, E-mail: rebane@physics.montana.edu)

Received: 27 April 1999/Published online: 11 August 1999

Abstract. We perform comprehensive theoretical and experimental analysis of ultrafast noncollinear and collinear parametric generation and amplification in type-I phase-matched BBO crystal, pumped with 390 nm wavelength, 150-fs-duration pulses from a frequency-doubled regenerative-amplified Ti:sapphire laser. We investigate conditions for group-velocity-matched generation and amplification, seeded with white-light continuum pulses by considering mean propagation velocity of pump and parametric pulses. We show that under certain conditions, effective matching can be achieved for noncollinear geometry with a 390-nm pump. We report detailed energy, spectral, and temporal measurement of the parametric processes in BBO and show that our effective matching conditions agree with experimentally observed angular and spectral properties of the parametric gain. The maximum tuning range for noncollinear process was from 460 nm to 2.56 μm, with the highest conversion efficiency of up to 20%. For collinear geometry, no effective matching of average group velocity was found. Because of this, the maximum conversion efficiency with UV pump in single-pass OPA is limited to 1.5%.

PACS: 42.65.Yj; 42.65.Re; 42.79.Nv

Optical parametric generation (OPG) and optical parametric amplification (OPA) are versatile methods for converting the wavelength of different pulsed laser sources into a broad spectral range from UV to far IR [1]. Because of availability of high-intensity fs pulses at Ti:sapphire laser wavelengths, in recent years there has been increasing interest in efficient parametric conversion of the energetic ultrashort pulses into the visible spectral range [2–10].

Among different nonlinear media, β-barium-borate has been most widely used because of its large nonlinear parametric coefficient, broad range of phase-matching wavelengths, and several other exceptional properties, such as high optical damage threshold and good optical quality [6, 11]. One possibility to achieve wavelength tuning in the visible, is by producing signal and idler from infrared fundamental pulses, followed by second-harmonic generation or sum-frequency generation in a separate nonlinear crystal [12]. To tune the wavelength in a broad range, it is necessary to adjust the phase-matching angle of two crystals simultaneously. In many applications the favoured way would be to use frequency-doubled output of the fs laser to directly convert it to the visible range.

If the parametric beams are collinear, then they interact over a longer propagation distance inside the crystal, as compared to beams propagating at different angles. For this reason, collinear parametric generation is typically more efficient and exhibits lower threshold than the corresponding noncollinear process. If the pump pulse duration is in the ps range or longer, then collinear OPG in BBO strongly prevails over any noncollinear generation.

For the fs pump pulses, however, a situation rather different from that described above can be encountered. For short pump pulses it is necessary to consider, in addition to the phase-velocity matching, also the matching of the group velocity with the propagation velocity of the parametric waves. Especially in nonlinear crystals with large dispersion, and for visible and ultraviolet wavelengths, the mismatch of the group velocities can change the parametric interaction in such way that the generation takes place preferentially in noncollinear direction, rather than in collinear direction.

Ultrafast parametric processes investigated so far have mostly sought to increase the efficiency of the collinear OPG and OPA by means of suppressing the accompanying noncollinear process. Several approaches such as seeding with white-light continuum pulses and multiple-pass amplification in two or more crystals have been used. Broadband noncollinear generation was recently used to produce, after compression, 16-fs pulses [8] and sub-10-fs pulses [13, 14]. Less attention has been devoted, however, to more systematic study of the relation between the collinear and noncollinear effects in BBO as well as in other nonlinear crystals.

In the present paper we present a comprehensive theoretical and experimental analysis of fs parametric generation and amplification in type-I phase-matched BBO crystal, pumped with 390 nm wavelength, both in noncollinear and collinear geometry. For excitation we use 150-fs-duration pulses from

frequency-doubled regenerative-amplified Ti:sapphire laser. We analyse theoretically the conditions for group-velocity-matched generation and amplification, seeded with white-light continuum pulses by considering mean propagation velocity of pump and parametric pulses. Our analysis shows that effective matching can be achieved for certain noncollinear geometries with 390 nm pump. In the experimental section we report detailed energy, spectral, and temporal measurement of the parametric processes in BBO. By comparing theoretical and experimental results we show that our effective matching conditions determine several of the observed angular and spectral features of the process.

1 Theoretical considerations

Let us consider a type-I optical parametric process, in which extraordinary polarized pump of frequency ω_p is propagating with wave vector $\boldsymbol{k}_\mathrm{p}$. The pump is generating ordinary polarized signal and idler waves with frequency ω_s and ω_i, such that $\omega_\mathrm{p} = \omega_\mathrm{s} + \omega_\mathrm{i}$. The condition for matching phase velocity is:

$$\boldsymbol{k}_\mathrm{p} = \boldsymbol{k}_\mathrm{s} + \boldsymbol{k}_\mathrm{i} \,, \tag{1}$$

where $\boldsymbol{k}_\mathrm{s}$ and $\boldsymbol{k}_\mathrm{i}$ are the wave vectors of the signal and idler wave, respectively. Figure 1 shows the relative orientation of the wave vectors with respect to the crystal axis, $\hat{C}$. The phase-matching angle θ_p between $\boldsymbol{k}_\mathrm{p}$ and $\hat{C}$ can be varied by rotating the crystal. In noncollinear geometry, there are two distinct propagation geometries of the parametric waves about the direction of the pump. In the first case $\theta_\mathrm{s} < \theta_\mathrm{i}$, i.e. the signal wave is propagating at a closer angle to the $\hat{C}$ axes than the idler (Fig. 1a), in the second case $\theta_\mathrm{s} > \theta_\mathrm{i}$ and the situation is reversed (Fig. 1b). Figure 1 shows also the direction of energy propagation (Poynting vector) for each of the three waves. The length of these vectors is proportional to the absolute value of group velocity of corresponding pulses. For the pump beam, in a birefringent nonlinear crystal the energy propagation direction differs from the wave vector by walk-off angle ρ, determined as [15]:

$$\rho = \mathrm{atan}\left[\left(\frac{n_\mathrm{po}}{n_\mathrm{pe}}\right)^2 \tan\theta_\mathrm{p}\right] - \theta_\mathrm{p} \,, \tag{2}$$

where n_po and n_pe are indices of refraction for ordinary and extraordinary polarized pump wave. In collinear parametric generation, the direction of wave vectors $\boldsymbol{k}_\mathrm{s}$ and $\boldsymbol{k}_\mathrm{i}$ coincides with the direction of the pump wave vector, which is a limit case of the present noncollinear interaction scheme.

The propagation angle θ_s is related to angle θ_p and indices of refraction for ordinary and extraordinary waves, according to:

$$\theta_\mathrm{s} = \theta_\mathrm{p} \mp \mathrm{acos} \frac{n_\mathrm{po}^2 n_\mathrm{pe}^2 (1+\beta)^2 + (n_\mathrm{so}^2 - \beta^2 n_\mathrm{io}^2)[n_\mathrm{pe}^2 + (n_\mathrm{po}^2 - n_\mathrm{pe}^2)(\sin\theta_\mathrm{p})^2]}{2(1+\beta) n_\mathrm{so} n_\mathrm{po} n_\mathrm{pe} \sqrt{n_\mathrm{pe}^2 + (n_\mathrm{po}^2 - n_\mathrm{pe}^2)(\sin\theta_\mathrm{p})^2}} \,. \tag{3}$$

where $\beta = \lambda_\mathrm{s}/\lambda_\mathrm{i}$ is the ratio between the wavelengths of the signal and the idler waves inside the crystal. Minus (plus) sign in front of acos corresponds to the beam geometry addressed in Fig. 1a,b. In a similar manner, the propagation angle of the idler wave θ_i is found to be:

$$\theta_\mathrm{i} = \theta_\mathrm{p} \mp \mathrm{acos} \frac{n_\mathrm{po}^2 n_\mathrm{pe}^2 (1+\beta)^2 - (n_\mathrm{so}^2 - \beta^2 n_\mathrm{io}^2)[n_\mathrm{pe}^2 + (n_\mathrm{po}^2 - n_\mathrm{pe}^2)(\sin\theta_\mathrm{p})^2]}{2\beta(1+\beta) n_\mathrm{io} n_\mathrm{po} n_\mathrm{pe} \sqrt{n_\mathrm{pe}^2 + (n_\mathrm{po}^2 - n_\mathrm{pe}^2)(\sin\theta_\mathrm{p})^2}} \,, \tag{4}$$

Figure 2 shows the phase-matching angles and parametric wavelengths in BBO crystal, when the pump wavelength is 390 nm. Here we used (1)–(4), and tabulated refraction index data and Sellmeier equation from [11]. The dashed line corresponds to signal and idler waves collinear to the pump. The crosshatched area shows the phase matching for noncollinear geometry, where all three waves can propagate in different directions. The range of parametric wavelengths shown in Fig. 2 is restricted from above due to strong absorption of the idler wave at $\lambda > 2.6\,\mu$m caused by intrinsic infrared absorption of the BBO crystal.

For collinear phase matching, to every angle in the interval, $\theta_\mathrm{p} = 23°$–$30°$, there corresponds a specific signal wavelength in the interval 460–780 nm, and a respective specific idler wavelength in the interval 2.56 μm to 780 nm. For non-

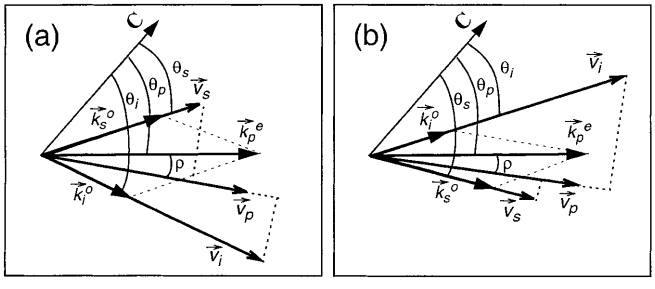

Fig. 1. Orientation with respect to the crystal axis of wave vectors and energy propagation vectors for pump, signal, and idler. The length of energy propagation vector is proportional to the absolute value of corresponding group velocity

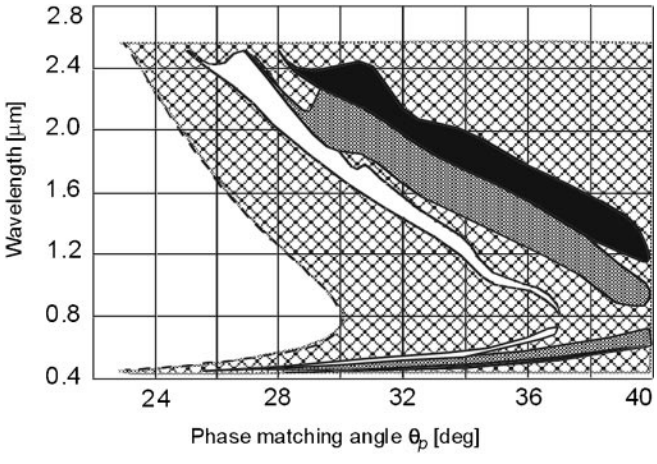

Fig. 2. Matching conditions for type-I parametric process in BBO at 390-nm pump wavelength. Phase matching for collinear OPG (*dash line*). Phase matching for noncollinear OPG (*cross-hatch area*). Effective group-velocity matching between pump and signal (*dark shaded areas*); pump and idler (*unshaded area*); pump and average of idler and signal (*lightly shaded area*)

collinear phase matching, however, there is no one-to-one correspondence between θ_p and generated wavelengths. For each phase-matching angle θ_p there are many possible signal and idler wavelengths, generated at different angles θ_s and θ_i. For any particular value of θ_p, $> 30°$, it is possible to generate the whole parametric spectrum, covering the entire interval between 460 nm and 2.56 μm. In this case, different wavelengths are produced at a variety of different angles θ_s and θ_i, centered around the pump beam direction, giving rise to characteristic cone-shaped beams. From the side of small angles, the noncollinear region is restricted by the collinear curve. As the angle approaches $\theta_p = 23°$, the range of allowed wavelengths gradually narrows down to 460 nm and 2.6 μm for the signal and idler wave, correspondingly. From the large-angles side, the noncollinear phase matching is possible up to $\theta_p = 90°$.

As we have pointed out in the introduction, in order to obtain a complete picture of frequency conversion of fs pulses, we need to consider mismatch between group velocity of the pump pulse and the parametric pulses. For a pulse of center wavelength λ, the group velocity is given as:

$$v = \frac{c}{n}\left(1 + \frac{\lambda}{n}\frac{\mathrm{d}}{\mathrm{d}\lambda}n(\lambda)\right) , \tag{5}$$

where $n(\lambda)$ is wavelength-dependent index of refraction of the media. Pulses propagating in different directions and with different polarizations will experience different dependences, $\mathrm{d}/(\mathrm{d}\lambda)n(\lambda)$. In particular, for extraordinary polarized pump pulse propagating at θ_p:

$$\frac{\mathrm{d}}{\mathrm{d}\lambda}n^{\mathrm{e}}(\lambda) = \frac{\frac{\mathrm{d}n^{\mathrm{e}}}{\mathrm{d}\lambda}n_{\mathrm{e}}^3(\cos\theta_p)^2 + \frac{\mathrm{d}n_{\mathrm{e}}}{\mathrm{d}\lambda}n_{\mathrm{o}}^3(\sin\theta_p)^2}{[(n_{\mathrm{o}}^2 - n_{\mathrm{e}}^2)(\sin\theta_p)^2 + n_{\mathrm{e}}^2]^{3/2}} . \tag{6}$$

Figure 3 shows the difference of inverse group velocities between the 390-nm pump pulse and the parametric pulses in collinear geometry, as a function of signal and idler wavelength. We see that this difference is especially large between the pump and idler. For example, 150-fs-duration pulses will walk off after as little as 0.5 mm propagation length. This is, as we think, the primary reason for small conversion efficiency for ultrashort pulses in BBO in the visible range. We note that in the longer wavelength range, for example for fundamental wavelength of Ti:sapphire laser around $\lambda_p = 800$ nm, the temporal walk off for collinear OPG is two orders of magnitude less than in UV, which permits collinear OPG even with ultrashort pulses [12].

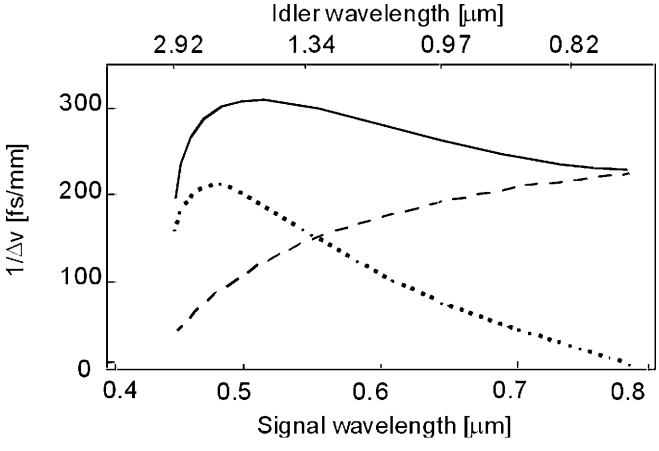

Fig. 3. Difference between inverse group velocities of 390-nm pump and parametric pulses as a function of signal and idler wavelength. Between pump and idler (*solid line*); Between pump and signal (*dashed line*); Between idler and signal (*dotted line*)

Unfortunately, for the 390-nm pump wavelength, all three group velocities cannot be matched, neither for collinear nor for noncollinear geometry. Nevertheless, for the noncollinear case we can investigate the effective matching condition, which considers the impact of mean pulse velocities. The effective matching condition consists then in equating the group velocity of the pump to the projection of the signal group velocity on the vector $\boldsymbol{v}_p$:

$$v_p = v_s \cos(\theta_p - \theta_n + \rho) . \tag{7}$$

Similar matching condition between the pump and idler is:

$$v_p = v_i \cos(\theta_p - \theta_i + \rho) , \tag{8}$$

and between the pump and average of signal and idler:

$$v_p = \frac{1}{2}[v_s \cos(\theta_p - \theta_s + \rho) + v_i \cos(\theta_i - \theta_p - \rho)] . \tag{9}$$

In Fig. 2, we have plotted the regions, where the respective effective matching conditions (7), (8), and (9) are fulfilled. The two areas, above and below 780 nm correspond to the idler and signal waves, respectively. For a given angle θ_p, conditions (7) and (8) allow a relatively narrow intervals of wavelengths ($\Delta\lambda_s < 30$ nm), whereas interval defined by condition (9) is several times broader. Moreover, condition (7) does not allow a phase-matching angle smaller than $\theta_p = 28°$, whereas condition (8) does not allow angles larger than $\theta_p = 37°$. According to condition (9), for phase-matching angles, $30° < \theta_p < 40°$, signal is generated in the very broad spectral range of $\Delta\lambda_s > 150$ nm.

Once the allowed phase-matching angles and wavelengths are determined, we can use (3) and (4) to evaluate the corresponding propagation directions of the parametric beams. For example, according to (9), we obtain $0° < |\theta_p - \theta_s| < 8°$ for signal wave direction, and $0° < |\theta_p - \theta_i| < 20°$ for the idler. Discussion of the spectra and propagation angles of the parametric waves will be continued in the following sections of this paper.

The theoretical considerations presented above allow us to make the following predictions about OPG in BBO using 390-nm fs pump pulses:

(a) Noncollinear parametric generation should have a higher efficiency and lower threshold than simple collinear generation process;
(b) The center wavelength of the noncollinear signal wave changes from 460 nm towards 760 nm as the phase-matching angle is tuned from 25° to 40°;
(c) The spectral width of the signal beam increases from a few nm at $\theta_p = 25°$, to up to 150 nm at $31° < \theta_p < 40°$;
(d) Around the degeneracy wavelength, in an interval 780 ± 10 nm, where effective group-velocity matching does not exist, the parametric generation will be very weak or absent.

2 Experimental results and discussion

The schematic of our experimental setup is shown in Fig. 4. The laser source was Clark MXR Model CPA-1000 Ti:sapphire regenerative-amplifier laser system. After frequency-doubling in a 0.5-mm-thick BBO crystal we obtained 150-fs-duration pulses with 0.3-mJ energy at 390 nm wavelength at 1 kHz repetition rate. For OPG/OPA we used a 2-mm-thick BBO type-I crystal, cut at $\theta = 30°$ (Casix Ltd.). Focusing of the pump beam was by 25-cm focal length lens. To produce white light continuum, we diverted a small fraction of the laser beam at the fundamental wavelength 780 nm and focused it into a 5-mm-thick block of fused silica. The continuum seed beam was collimated with a lens and then directed into BBO crystal at a variable delay with respect to the pump beam. In collinear geometry, the seed was applied in the same direction as the pump. For noncollinear geometry, the seed was applied at an angle α with respect to the pump beam, such that inside the crystal the propagation direction of the seed coincided either with θ_s or θ_i. We measured the energy, the spectrum, and the duration of the generated pulses by splitting the beams between an optical power meter, a grating spectrometer, and an autocorrelator.

In the first experiment we studied parametric generation by blocking the seed beam before the BBO crystal. Intense parametric waves were observed at the output of the crystal in the form of two concentric conical beams, centered around the propagation direction of the pump. The threshold of this noncollinear process was about 15 μJ per pump pulse. At the same time, even at the highest pump intensities up to the damage threshold of the BBO crystal $P \approx 300\,\mathrm{GW\,cm^{-2}}$, we did not detect any collinear parametric generation. Figure 5a,b,c show a brightly colored signal beam, projected onto a white screen behind the crystal. By varying the phase-matching angle θ_p, the center wavelength of the signal was tuned in the range $\lambda_s = 460$–760 nm. The observed tuning range and the spectral bandwidth of the signal wave were in good agreement with our calculations. Maximum energy conversion efficiency occurred at $\theta_p = 30°$–$32°$. With the pump pulse energy 50 μJ the integrated-over-the-entire-ring total energy of the signal and idler pulse was about 15 μJ, resulting in maximum energy conversion efficiency (total into both beams) 30%.

The tuning range of the idler wave was $\lambda_i = 2.42$ μm–802 nm. Unfortunately, because of poor infrared sensitivity of our photographic film, we were not able to picture the idler beam in Fig. 4. Instead, we observed the idler with an infrared viewing camera, whose sensitivity dropped beyond 1.2 μm. In the range $\lambda_i = 1.2$ μm–802 nm the idler beam had a slightly larger cone angle than the signal, which is consistent with (4).

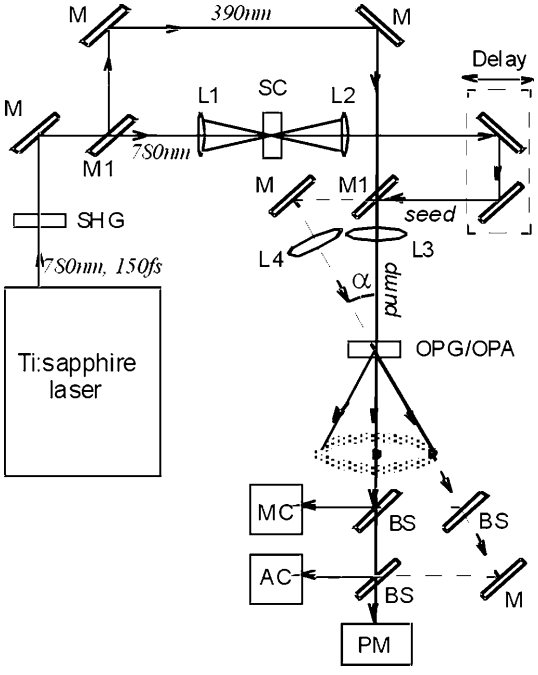

Fig. 4. Experimental setup. SHG, second-harmonic generator (BBO crystal); OPG/OPA, optical parametric generator/amplifier (BBO crystal); BS, beam splitter; M, mirror; M1, dichroic mirror; SC, glass plate for continuum generation; L, lens; AC, autocorrelator; PM, optical power meter; MC, grating monochromator

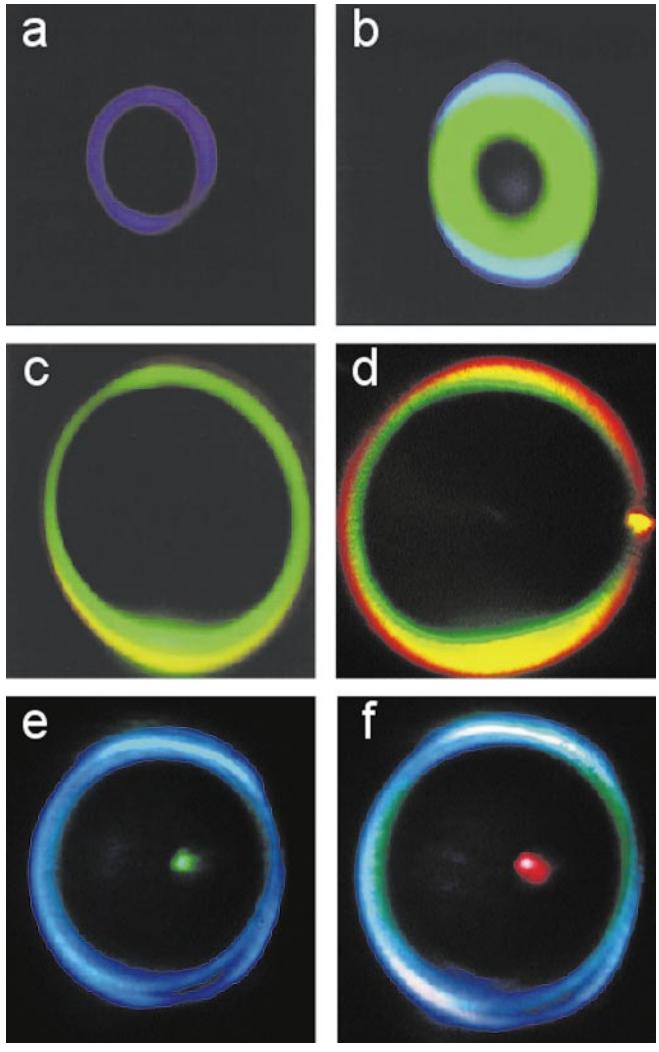

Fig. 5a–f. Photographed images of parametric signal wave at the output of the BBO crystal. **a** noncollinear spontaneous OPG at phase-matching angle $\theta_p = 25°$; **b** $\theta_p = 29°$; **c** $\theta_p = 31, 7°$; **d** noncollinear OPA with continuum seed at angle $\theta_s = 32.2°$; **e** collinear OPA at phase-matching angle $\theta_p = 25.5°$; **f** $\theta_p = 27.7°$

Figure 6 shows the spectrum of the signal at $\theta_p = 31.5°$, measured with pump energy slightly above the threshold (solid line) and with maximum pump energy five times above the threshold (dotted line). At low pump energy, both the observed center wavelength about $\lambda_s = 560$ nm as well as the width of the generated spectrum, $\Delta\lambda_s = 30$ nm agree well with theoretical prediction of matching condition (7). On the other hand, the broadening of the signal spectrum at higher pump energy can be explained by addition of the effective matching condition (8) and especially (9), which, according to Fig. 2 allow additional spectral components on the long wavelength side of the generated spectrum.

Unfortunately we, as other investigators, did not observed collinear generated signal with rotation BBO crystal around phase-matching angles and with the pump pulse energy up to the damage the crystal. This confirms the importance the group-velocity matching for fs OPG.

We can conclude that the strongest group-velocity matching requirement is that between the pump and the signal pulse, expressed by the condition (7). However, especially at pump energies well above the threshold, also two other conditions, (8) and (9), take effect.

In the next experiment we investigated the effect of the seed pulse on the noncollinear parametric gain and generation. When the seed beam was open, then we observed that the generation in the direction of the seed beam was strongly amplified. At the same time, the overall energy of the conical signal wave decreased by more than 50%. We note that to observe this effect, the direction and the delay of the seed pulse had to exactly coincide with the direction and the time delay of the signal wave. Figure 5d shows the bright spot due to noncollinear amplification at 560 nm. Figure 6 shows that in the case of OPA, the bandwidth of the signal wave was about 15 nm, which is a factor of two less than with OPG at the same pump energy. The duration of the amplified pulses was about 200 fs, without additional compression.

Figure 7 shows the change of the energy of OPA pulse, as the pump pulse energy was increased from 4 μJ to 50 μJ. The energy of the seed pulse was a constant 3×10^{-6} μJ. The wavelength of the OPA output was $\lambda_s = 560$ nm and was determined by the angle α, which was tuned to the

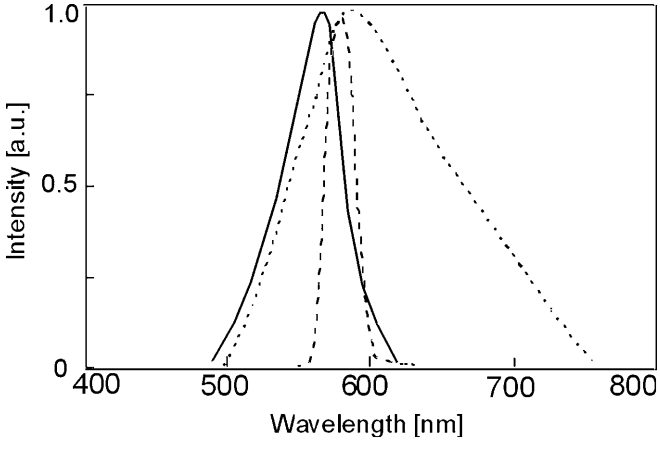

Fig. 6. Spectrum of signal pulses in noncollinear OPG for pump pulse energy 10 μJ (*solid line*) and 50 μJ (*dotted line*); spectrum of seeded OPA with 10-μJ pump (*dashed line*); phase-matching angle $\theta_p = 31.5°$

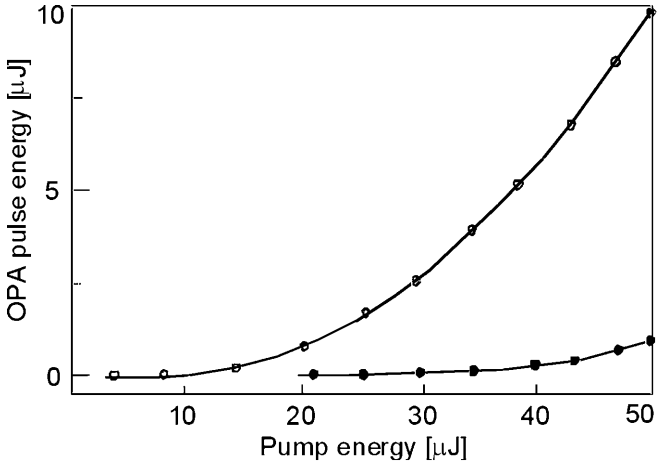

Fig. 7. Energy of OPA pulse produced at $\lambda_s = 560$ nm, measured as a function of pump pulse energy in collinear (*filled circles*) and noncollinear (*open circles*) geometry. The energy of the seed pulse is 3×10^{-6} μJ

corresponding signal amplification wavelength. Simultaneously with the amplification in the direction of the visible signal beam, an increased idler intensity was produced in the corresponding conjugated direction, at the corresponding near-infrared wavelength [10]. The threshold for noncollinear amplification was 8 μJ, which is about two times less that the threshold of OPG under similar excitation. From Figs. 6 and 7 we can further conclude that seeding not only reduces the threshold of the noncollinear generation, but also increases the brightness of the signal wave, by increasing its energy and by narrowing its spectral width and, especially, by greatly reducing the beam divergence. In addition, the seeded parametric process yields an improved pulse-to-pulse energy stability and a better spatial beam quality than spontaneous OPG in the same configuration.

By choosing angle α such that the seed beam became parallel to the idler beam direction, we were able to efficiently amplify the near-infrared portion of the seed pulses. As expected, the amplification in the infrared was accompanied by production of intense visible beam in the corresponding signal direction. We measured the amplification factor for weak near-infrared seed pulses with energy about 10^{-16} J, and obtained values on the order 10^9, which is comparable to the amplification factors measured earlier for seed in the signal beam direction [10]. It is interesting to mention that our experimental technique can be used for cross-correlation measurement of time profile of weak ultrashort pulses in near-infrared range.

As the last step, we investigated collinear OPA by setting the seed beam propagation direction to coincides with the direction of the pump. Figure 5e,f show images produced by the amplified seed at two phase-matching angles $\theta_p = 25.5°$ and $\theta_p = 27.7°$. We were able to angle-tune the center wavelength in the interval 460–700 nm, while the width of the amplified spectrum changed from 13 nm to 22 nm. The amplified pulse duration at 560 nm was 150 fs. Note that the collinear OPA is accompanied by a distinctive circle pattern of noncollinear OPG. This again confirms that the noncollinear process has a much higher gain that the collinear interaction. Figure 5 shows that even at the wavelength of maximum parametric gain $\lambda_s \approx 560$ nm the collinear amplification factor is by an

order of magnitude less than the corresponding amplification for noncollinear seed beam.

3 Conclusion

To summarize, we have analyzed interrelation between noncollinear and collinear parametric generation and amplification in type-I phase-matched BBO crystal, pumped by UV 150-fs-duration pulses. Our results give consistent quantitative explanation to the observation that at UV pump wavelengths, noncollinear parametric process tends to prevail over collinear interaction. The maximum tuning range for noncollinear process was from 460 nm to 2.56 μm, with the highest conversion efficiency of up to 20%, as opposed to 1.5% maximum efficiency for collinear case. The theoretical analysis revealed conditions for effective group-velocity matching, taking into account mean propagation velocity of pump- and parametric pulses. We have used these effective group-velocity-matching conditions to amplify white light continuum seed pulses both, in the visible and in the infrared range of wavelengths. In the last case, noncollinear amplification in an infrared idler beam, produces a visible signal beam.

References

1. R.L. Bayer, A. Piskarskas: J. Opt. Soc. Am. B **10**, 1659 (1993)
2. J. Watson, T. Lépine, P. Georges, B. Alonzi, A. Brun: Opt. Lett. **19**, 231 (1994)
3. V. Krylov, A. Kalintsev, A. Rebane, D. Erni, U. Wild: Opt. Lett. **20**, 151 (1995)
4. S.R. Greenfield, M.R. Wasielewski: Opt. Lett. **20**, 1394 (1995)
5. P. Di Trapani, A. Andreoni, P. Foggi, C. Solcia, R. Danielius, A. Piskarskas: Opt. Commun. **119**, 327 (1995)
6. M.K. Reed, M.K. Steiner-Shepard, M.S. Armas, D.K. Negus: J. Opt. Soc. Am. B **12**, 2229 (1995)
7. P. Di Trapani, A. Andreoni, C. Solcia, G.P. Banfi, R. Danelius, A. Piskarskas, P. Foggi: J. Opt. Soc. Am. B **14**, 1245 (1997)
8. T. Wilhelm, J. Piel, E. Riedle: Opt. Lett. **22**, 1494 (1997)
9. A. Shirakawa, T. Kobayashi: Appl. Phys. Lett. **72**, 147 (1998)
10. V. Krylov, O. Ollikainen, J. Gallus, U. Wild, A. Rebane, A. Kalintsev: Opt. Lett. **23**, 100 (1998)
11. *Crystal Guide 97/98, Crystals & Materials*. Fuzhou, Fujian, P.R. China: CASIX Inc. 1998
12. P. Di Trapani, A. Andreoni, C. Solcia, D. Podenas, R. Danelius, A. Piskarskas: Appl. Opt. **35**, 5336 (1996)
13. G. Gerullo, M. Nisoli, S. Stagira, S. De Silvestri: Opt. Lett. **23**, 1283 (1998)
14. A. Shirakawa, I. Sakane, T. Kobayashi: Opt. Lett. **23**, 1292 (1998)
15. V.G. Dmitriev, G.G. Gurzadyan, D.N. Nikogosyan: *Handbook of Nonlinear Optical Crystals* (Springer, Berlin, Heidelberg 1997)